# Strongly Interacting C$_{60}$/Ir(111) Interface: Transformation of C$_{60}$ into Graphene and Influence of Graphene Interlayer

Xiangmin Fei,[†,‡] Xu Zhang,[‡] Vanessa Lopez,[‡] Gang Lu,*[,‡] Hong-Jun Gao,[†] and Li Gao*[,‡]

[†]Institute of Physics, Chinese Academy of Sciences, Beijing 100190, China

[‡]Department of Physics and Astronomy, California State University, Northridge, California 91330, United States

S *Supporting Information*

ABSTRACT: The adsorption, electronic structure, and thermodynamics of C$_{60}$ molecules on Ir(111) and graphene/Ir(111) surfaces have been investigated by combining scanning tunneling microscopy and spectroscopy as well as density functional theory calculations. C$_{60}$ is found to interact strongly with the Ir surface, leading to a spontaneous formation of graphene on the Ir surface at elevated temperatures. The introduction of a graphene interlayer at the C$_{60}$/Ir(111) interface dramatically affects the interface properties, including the formation of larger molecular islands, improvement in ordering of molecular arrangements, suppression of charge transfer between C$_{60}$ and Ir, and thermal desorption of C$_{60}$ from the surface without decomposition or polymerization. We also find that C$_{60}$ is an effective solid precursor for preparing small-sized graphene quantum dots as well as graphene layers on the Ir surface.
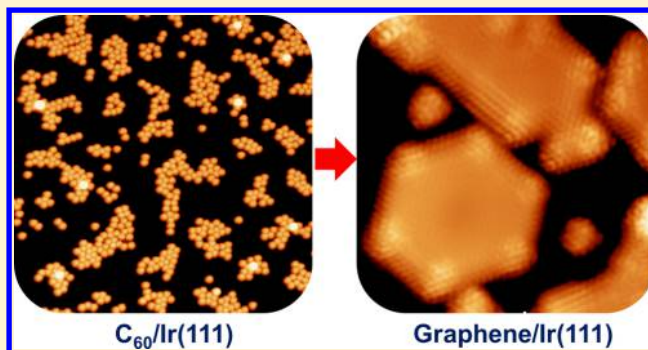
1. INTRODUCTION

Fullerene (C$_{60}$) molecules exhibit a great potential for applications in electronics, spintronics, optoelectronics, photocatalysis, and hydrogen storage.[1−9] The properties of interfaces between C$_{60}$ molecules and metal electrodes play a critical role in these applications and hence have been the focus of extensive research in recent years. The C$_{60}$/metal interfaces can be classified into three categories depending on the strength of interfacial interaction and the behavior of C$_{60}$ at elevated temperatures. Upon thermal annealing, for strongly interacting interfaces, such as C$_{60}$/Ru, C$_{60}$/Ni, and C$_{60}$/Pt, C$_{60}$ molecules would decompose and form graphene;[10−13] for intermediately interacting interfaces, such as C$_{60}$/Cu and C$_{60}$/Ag, C$_{60}$ molecules would polymerize;[13,14] and for weakly interacting interfaces, such as C$_{60}$/Au and C$_{60}$/Pd, C$_{60}$ molecules would simply desorb without decomposition or polymerization.[15,16] Because iridium (Ir) is one of the most commonly used electrode materials, it is of scientific and technological importance to examine the properties of the C$_{60}$/Ir interface, which remain largely unknown up to now.

Additionally, coating metal surfaces with graphene has attracted much attention recently thanks to the remarkable chemical inertness and thermal properties of graphene.[17−25] Graphene coatings can effectively enhance the metals' resistance to oxidation and corrosion, improve heat dissipation in electronic devices, and strengthen the stability of the devices in harsh environments.[17−25] It has been noted that the graphene interlayer could affect the interaction of molecules with metal surfaces.[26−30] Hence it would be interesting to investigate how the graphene interlayer would influence adsorption, electronic structure, and thermodynamics of C$_{60}$ molecules on the Ir surface.

Herein, we report our investigations of C$_{60}$ molecules on Ir(111) and graphene/Ir(111) surfaces employing scanning tunneling microscopy (STM), scanning tunneling spectroscopy (STS), and density functional theory (DFT) calculations. Upon deposition at room temperature, C$_{60}$ molecules aggregate into small disordered clusters on Ir(111), while they assemble into large ordered islands on the graphene/Ir(111) surface. A zero-conductance gap is observed for C$_{60}$ on graphene/Ir(111) but not on Ir(111). Upon thermal annealing, C$_{60}$ molecules decompose and transform into graphene on Ir(111), indicating a strong interfacial interaction for C$_{60}$/Ir. In contrast, C$_{60}$ molecules desorb from the graphene/Ir(111) surface at elevated temperatures without decomposition or polymerization, indicative of a weak interfacial interaction. DFT calculation reveals charge transfer from the Ir surface to C$_{60}$, which can be significantly reduced by the graphene interlayer. Finally, C$_{60}$ is found to be an effective solid precursor for preparing small-sized graphene quantum dots (GQDs) as well as graphene layers on the Ir(111) surface.

2. EXPERIMENTAL AND THEORETICAL METHODS

All experiments were performed using a Unisoku ultrahigh vacuum (UHV) low-temperature STM system (USM1500S) with a base pressure lower than 2×10^{-10} Torr. The single-crystal Ir(111) surface (Princeton Scientific) was cleaned by repeated cycles of Ar^+ ion sputtering and subsequent flash annealing to ~1500 K. After that, the sample was annealed first in oxygen (1×10^{-7} Torr, 20 min) and then in hydrogen (5×10^{-7} Torr, 20 min) at ~1200 K to remove residual impurities on the surface. For the convenience of investigating the influence of the graphene interlayer on the properties of C_{60} molecules on the surface, submonolayer graphene was grown on Ir(111) by exposing the Ir surface to ethylene (1×10^{-7} Torr) at 1350 K for 1 min and subsequently annealing at 1250 K for 10 min. The deposition of C_{60} molecules (sublimed grade, 99.9%, Sigma-Aldrich) was performed by thermal evaporation at ~590 K from an Al_2O_3 crucible. The C_{60} molecules were thoroughly degassed prior to molecular deposition. The substrate was held at room temperature during molecular deposition. All STM and STS measurements were performed at 77 K with tungsten tips prepared by electrochemical etching. In this work, the same Ir(111) single crystal was used, and the absolute orientation of the single crystal in the microscope is the same for all measurements here. The differential conductance (dI/dV) spectra were recorded using a lock-in technique with a small ac modulation signal (853 Hz, 20 mV).

In our DFT calculations, we used a $9 \times 9(\sqrt{3} \times \sqrt{3})R30°$ unit cell for the Ir(111) surface. A four-layer slab was used in these calculations with the top two layers fully relaxed. To model the graphene/Ir substrate, we place a monolayer graphene with 10×10 unit cells over 9×9 Ir(111) surface unit cells; such interface yields a moiré pattern with a repeat distance of 2.53 nm, in good agreement with experiments.[31] For the adsorption of a C_{60} molecule on the substrate, the most stable structure was found to be a three-fold axis of the C_{60} molecule coinciding with a three-fold axis of the substrate surface.[32] DFT calculations were carried out using the VASP package[33] with the projector-augmented wave pseudopotentials[34] and Perdew−Burke−Ernzerhof generalized gradient approximation.[35] An energy cutoff of 400 eV was used for the plane-wave basis set. Because of the large size of supercell, only Γ-point was considered in the Brillouin zone, which had been tested to yield the converged results. The van der Waals interaction is described by semiempirical DFT-D2 scheme of Grimme,[36] and the C_6 coefficients of C and Ir are chosen to be 1.75 and 81.24 J × nm^6/mol, respectively.[36,37] The force convergence criterion for atomic relaxation is 0.02 eV/Å.

3. RESULTS AND DISCUSSION

3.1. Influence of the Graphene Interlayer on the Adsorption of C_{60} Molecules on the Surface.
A clean Ir(111) surface was first coated with submonolayer graphene and then decorated with 0.35 monolayer (ML) of C_{60} molecules. Figure 1a shows an atomic-resolution STM image of graphene on Ir(111). The STM image in Figure 1b was recorded crossing the boundaries between the C_{60}/Ir(111) and C_{60}/graphene/Ir(111) regions. A strong contrast in C_{60} adsorption between the two regions is clearly visible. On the Ir(111) surface, C_{60} tends to aggregate into smaller and disordered clusters with dimensions below 15 nm, as shown in Figure 1b,c; some of the C_{60} molecules end up at the second
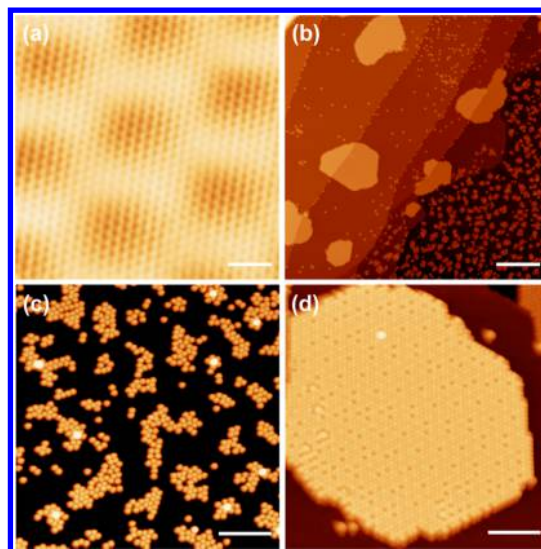
Figure 1. (a) Atomic-resolution STM image of graphene on Ir(111). (b) STM image showing both the C_{60}/Ir(111) (lower right) and C_{60}/graphene/Ir(111) (upper left) regions. (c) STM image of small C_{60} clusters formed on Ir(111). (d) STM image of large C_{60} islands formed on graphene/Ir(111). Scanning parameters: (a) V_{bias} = 20 mV, I = 8 nA; (b) V_{bias} = 3 V, I = 10 pA; (c) V_{bias} = 2 V, I = 100 pA; and (d) V_{bias} = 3 V, I = 50 pA. Scale bars: (a) 1; (b) 50; (c) 10; and (d) 10 nm.

molecular layer. The number density of the clusters is ~2×10^4 μm^{-2}. On the graphene/Ir(111) surface, C_{60} molecules assemble into larger and ordered islands with sizes ranging from 20 to 80 nm, as shown in Figure 1b,d. The number density of the islands varies from (1 to 5) × 10^2 μm^{-2}. Single C_{60} vacancies are formed in most of the islands with a quasi-periodic pattern, as shown in Figure 1d, which tracks the underlying moiré pattern. The moiré pattern has been found an efficient template for the growth of a C_{60} superstructure on the graphene/Ru(0001) surface.[38] Two types of vacancy super-lattice were observed in our samples (see Supplementary Figure S1), correlated with two different moiré patterns on the underlying graphene/Ir(111) surface. In weakly interacting graphene/metal systems, multiple different graphene domains with varied moiré patterns coexist.[39,40] We have observed different graphene domains on our graphene/Ir(111) sample surface (see Supplementary Figure S2). Interestingly, we find that the transition between the molecular arrangement with vacancies and the one without vacancies always occurs at the boundaries between different domains on the underlying graphene/Ir(111) surface (see Supplementary Figure S3). This suggests that the formation of the vacancies is closely related to the underlying graphene domains, that is, their moiré patterns.

Our observations indicate that the graphene interlayer has strong impacts on the adsorption of C_{60} molecules on the surface. On the Ir(111) surface, the adsorption is dominated by the molecule−substrate interaction, leading to a high density of nucleation sites and disordered molecular arrangements. On the graphene/Ir(111) surface, however, the adsorption is dominated by intermolecular interaction, resulting in a low density of nucleation sites and ordered molecular arrangements. The orientation of graphene lattice relative to the Ir(111) lattice affects the interaction of C_{60} with the graphene/Ir(111) surface. In most graphene domains, the moiré pattern leads to

the formation of vacancies in molecular islands, while in other graphene domains, the moiré pattern has negligible effect on molecular self-assembly, resulting in the formation of molecular islands with no vacancies.

3.2. Influence of the Graphene Interlayer on the Electronic Structure of C_{60} Molecules on the Surface.

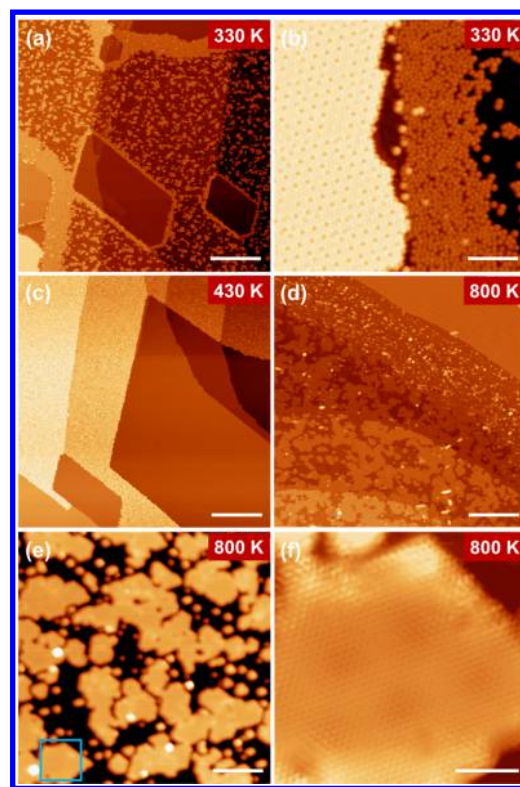Figure 2 shows the $I-V$ and dI/dV spectra measured for C_{60}
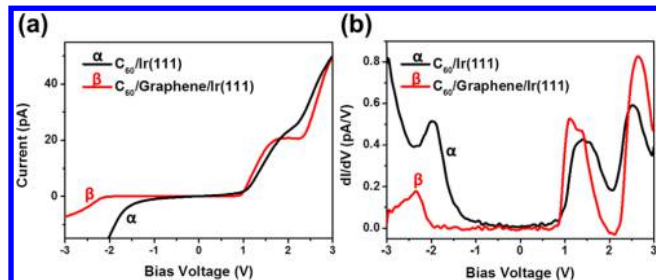
Figure 2. STS of C_{60} molecules on Ir(111) and graphene/Ir(111) surfaces. Stabilization conditions: $V_{bias} = 3$ V, $I = 50$ pA.

molecules on the Ir(111) and graphene/Ir(111) surfaces. On the Ir(111) surface, the HOMO, LUMO, and LUMO+1 levels are centered at −2.0, +1.4, and +2.5 eV, respectively. At the Fermi energy, E_F, the tunneling current changes linearly with bias voltage, indicating a metallic density of states (DOS). Thus, the electronic structure of C_{60} is modified by the underlying Ir(111) substrate. In comparison with the STS of C_{60}/Ir(111), the STS of C_{60} molecules adsorbed on graphene/Ir(111) exhibit two major differences. First, there is a zero-conductance gap of ∼2.9 eV, from around −2.0 eV to around +0.9 eV, between the HOMO and LUMO levels. Second, the molecular levels are centered around −2.3 eV for HOMO, +1.1 eV for LUMO, and +2.6 eV for LUMO+1, respectively. Hence the graphene interlayer strongly affects the electronic structure of C_{60} on the surface. In particular, the appearance of a zero-conductance gap between the HOMO and LUMO levels upon the insertion of the graphene interlayer indicates that C_{60} molecules interact very weakly with the graphene/Ir(111) surface when compared with the Ir(111) surface.

3.3. Influence of the Graphene Interlayer on the Thermodynamics of C_{60} Molecules on the Surface.

Figure 3a shows an STM image of the sample surface after thermal annealing at ∼330 K for 30 min. The scenario in the Ir(111) regions far from the borders remains the same as before annealing, which indicates that C_{60} molecules are not mobile on the Ir(111) surface at 330 K. One major change to the surface is that more molecules appeared around the boundaries between the Ir(111) and graphene/Ir(111) regions, which results from the diffusion of C_{60} molecules from the graphene/Ir(111) regions into the Ir(111) regions. These molecules stopped diffusion once they were in contact with the Ir(111) surface, and thus they formed a densely packed molecular layer starting from the boundaries, as shown in Figure 3b. This diffusion process is corroborated by our quantitative analysis of multiple STM images (see Supplementary Figure S4). Figure 3c shows an STM image of the surface after further annealing at ∼430 K for 30 min. We can see that many more C_{60} molecules diffused from the graphene/Ir(111) regions to the Ir(111) regions. No molecules were observed in the graphene/Ir(111) regions. The molecular arrangements in the Ir(111) regions remain disordered. These observations strongly indicate that it is much easier for C_{60} molecules to diffuse on the graphene/

Figure 3. STM images of the C_{60}/Ir(111) and C_{60}/graphene/Ir(111) regions after thermal annealing at (a,b) 330 K for 30 min, (c) 430 K for 30 min, and (d−f) 800 K for 30 min. The atomic-resolution STM image in panel f was recorded in the region indicated by the square in panel e. Scanning parameters: (a−d) $V_{bias} = 3$ V, $I = 50$ pA; (e) $V_{bias} = 2$ V, $I = 50$ pA; and (f) $V_{bias} = 10$ mV, $I = 9$ nA. Scale bars: (a) 40; (b) 10; (c) 40; (d) 40; (e) 10; and (f) 2 nm.

Ir(111) surface than on the Ir(111) surface. After further annealing at 800 K for 30 min, all adsorbed C_{60} molecules disappeared and many patches with flat surfaces formed in the Ir(111) regions, as shown in Figure 3d,e. Most of small patches are hexagonal. Although large patches do not have regular shapes, many of their edges are along one of three equivalent directions. High-resolution STM measurements revealed that graphene patches formed on the Ir(111) surface, as shown in Figure 3f. Thus, C_{60} molecules decomposed and transformed into graphene on the Ir(111) surface at this temperature. The intermediate structures between C_{60} and graphene were observed around the boundaries of the graphene patches (see Supplementary Figure S5a), which indicates that C_{60} molecules were involved in the formation of graphene patches.

Therefore, C_{60}/Ir can be classified as a strongly interacting interface because C_{60} molecules decomposes on the Ir surface at elevated temperatures, while the interface between C_{60} and the graphene/Ir(111) surface can be classified as a weakly interacting interface because C_{60} molecules desorb, without decomposition or polymerization, from the graphene/Ir(111) surface at elevated temperature. So the insertion of the graphene interlayer significantly promotes the diffusion of molecules on the surface and prevents the chemical reactions between molecules and the Ir surface.

3.4. DFT Calculations of C_{60} Molecules on the Ir(111) and Graphene/Ir(111) Surfaces.

DFT calculations were performed to provide quantitative pictures for the C_{60}/Ir and C_{60}/graphene/Ir(111) interfaces. We find that the binding

energy of a C_{60} molecule on the Ir(111) surface is 7.67 eV, and that the strong C_{60}-Ir binding stems from a significant charge transfer from the Ir(111) surface to the C_{60} molecule, as shown in Figure 4a. This result is consistent with the fact that C_{60} is a
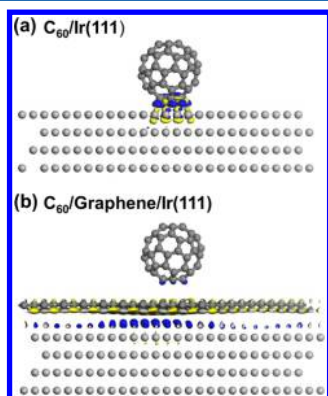

Figure 4. DFT simulations of C_{60} molecules on (a) Ir(111) and (b) graphene/Ir(111). The calculations show a significant charge transfer for C_{60} on Ir(111), while the C_{60} molecules are quasi-free on the graphene/Ir(111) surface with negligible charge transfer.

superior electron acceptor,[41] with a higher electronegativity than Ir. In contrast, the charge transfer between C_{60} and the graphene/Ir(111) surface is negligible, as shown in Figure 4b, and the interaction between C_{60} and the graphene/Ir(111) surface is of weak van der Waals nature.[42] To understand the correlation between C_{60} vacancies formation and the underlying moiré pattern, we have calculated the binding energy of a C_{60} molecule at two different adsorption sites, one with the largest interplanar distance between the graphene and Ir(111) surface (atop site) and the other with the smallest distance (fcc site). The corresponding binding energy is 1.27 eV for the fcc site and 1.17 eV for the atop site, respectively. Hence, C_{60} prefers to occupy the fcc site, and conversely C_{60} vacancies may prefer to be formed at the atop sites. This may explain the correlation between the C_{60} vacancy pattern and the underlying moiré superstructure, as observed in our experiments. Next, to understand the STS results, we have calculated the DOS of C_{60} on Ir(111) and graphene/Ir(111) surfaces (see Supplementary Figure S6). With C_{60} on the Ir(111) surface, the DOS at the Fermi energy does not vanish, which is consistent with the STS result. Moreover, we observe charge transfer from Ir to C_{60}, as shown in Figure 4a. In contrast, as the graphene interlayer is inserted between C_{60} and Ir(111), there appears a zero-conductance gap in DOS. Moreover, the partial DOS owing to C_{60} resembles closely that of a stand-alone C_{60} molecule, indicative of negligible electronic interaction or charge transfer between C_{60} and the graphene/Ir(111) substrate. These calculations are in qualitative agreement with our STS measurements and can explain the contrasting behaviors of C_{60} molecules on the two surfaces.

3.5. Synthesis of Graphene Layers on Ir(111) by Thermal Decomposition of C_{60} Molecules.
The observed transformation of C_{60} molecules into graphene on Ir(111) represents a new approach to synthesizing graphene on the Ir surface. C_{60}, as a solid precursor, is advantageous in growing well-defined graphene quantum dots and controlling graphene coverage.[11] The transformation of C_{60} into graphene was previously observed on Ru, Ni, and Pt surfaces.[10−13] Our observations indicate that such a transformation can also occur

on the Ir surface, where Ir acts as the catalyst for the cage-opening of C_{60}.

Figure 5a,b shows large-scale STM images of the surface after annealing 0.1 ML C_{60} molecules on Ir(111) at 780 K for 30
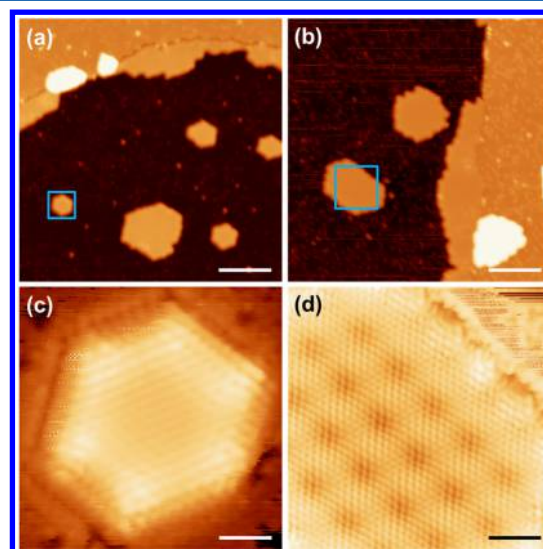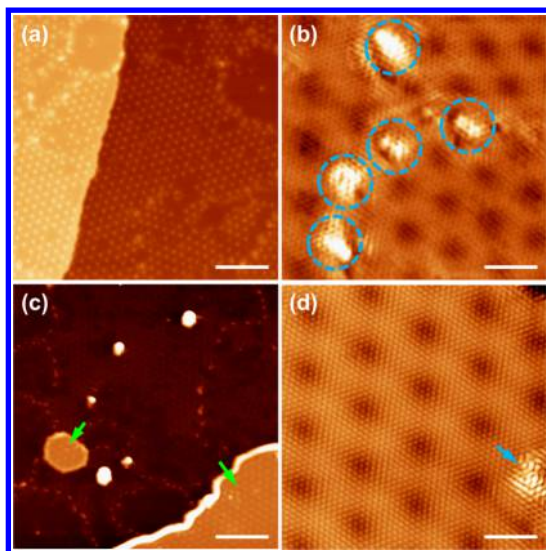

Figure 5. STM images of graphene patches obtained by thermal annealing 0.1 ML C_{60} molecules on Ir(111). The atomic-resolution STM images in panels c and d were recorded in the regions marked with a square in panels a and b, respectively. Different orientations of graphene lattice were observed for the graphene patches, as demonstrated by the atomic-resolution STM images. Scanning parameters: (a) V_{bias} = 2 V, I = 50 pA; (b) V_{bias} = 2 V, I = 50 pA; (c) V_{bias} = 200 mV, I = 5 nA; and (d) V_{bias} = 100 mV, I = 5 nA. Scale bars: (a) 10; (b) 10; (c) 1; and (d) 1.6 nm.

min. We can see that there are many graphene patches, which are of different size and shape, dispersed on the surface. Smaller patches tend to have well-defined hexagonal shapes while larger patches tend to exhibit irregular shapes. In addition, we found that the orientation of graphene lattice is not exactly the same for all patches as different moiré patterns were observed for these patches. Figure 5c,d shows two atomic-resolution STM images of graphene patches, showing two distinct moiré patterns. In Figure 5c, the orientation of graphene lattice is parallel to the edges of the graphene patch. In Figure 5d, however, the orientation of graphene lattice is not parallel to the edges of the graphene patch. It is worth mentioning that most of the smallest graphene patches are in the form of hexagonal GQDs with a size of ∼4 nm, as shown in Figure 5a. Our further experiments show that the smallest size of the GQDs obtained by thermal decomposition of ethylene (C_2H_4) is ∼10 nm (see Supplementary Figure S7). Such difference between C_{60} and C_2H_4 was also observed on Ru(0001).[11] Our observations indicate that C_{60} is an efficient precursor for preparing small-sized GQDs on Ir(111).

Figure 6 shows the scenario when additional 0.6 ML C_{60} molecules were deposited onto the surface and subsequently annealed to 1300 K. A full monolayer of graphene was obtained on the surface, as shown in Figure 6a. Multiple different domains were observed in the obtained graphene layer. Different domains can be distinguished by different moiré patterns. When scanning the surface with a bias voltage of 3 V and a tunneling current of 50 pA, the moiré patterns are observable in some domains but not in other domains, as shown in Figure 6a. The moiré patterns in all domains can be

Figure 6. STM images of graphene obtained by thermal annealing 0.7 ML C_{60} molecules on Ir(111). (a) Different graphene domains with varied moiré patterns coexist in the graphene layer. (b) Atomic-resolution STM image of the boundaries between three different graphene domains. The graphene lattices in these three domains are different from each other, leading to different moiré patterns. (c) Bilayer graphene islands formed on the surface. (d) Atomic-resolution STM image of the bilayer graphene. The feature indicated by the arrow is the electron-scattering pattern around a defect. Scanning parameters: (a) V_{bias} = 3 V, I = 50 pA; (b) V_{bias} = 10 mV, I = 5 nA; (c) V_{bias} = 2 V, I = 50 pA; and (d) V_{bias} = 10 mV, I = 5 nA. Scale bars: (a) 13; (b) 2; (c) 16; and (d) 2 nm.

clearly resolved when scanning the surface with a bias voltage of 10 mV and a tunneling current of 5 nA. Figure 6b shows an atomic-resolution STM image recorded across the boundaries between three different domains. It is clear that the graphene lattice orientation, and thus the moiré pattern, is different between these domains. At the domain boundaries, we did not observe obvious electron scattering patterns. There are bright protrusions arranged with roughly equal spacing along the domain boundaries, as indicated by dashed circles in Figure 6b. These bright protrusions can be used to identify the domain boundaries on the surface from large-scale STM images. We also observed bilayer graphene islands on the surface, as indicated by arrows in Figure 6c. The atomic-resolution STM image of bilayer graphene is shown in Figure 6d. One unique feature of bilayer graphene compared with single-layer graphene on the Ir(111) surface is that the point defects in bilayer graphene lead to intervalley scattering patterns, as indicated by the arrow in Figure 6d. There are two possible mechanisms for the formation of bilayer graphene, either by the segregation of carbon atoms from the Ir substrate or by the decomposition of C_{60} molecules. In our experiments, we observed the intermediate structures between C_{60} and graphene at the edges of bilayer graphene islands (see Supplementary Figure S5b), which indicates that C_{60} molecules are involved in the formation of bilayer graphene islands. Recently Nie et al. observed that the second graphene layer on Ir(111) nucleates and grows below the first graphene layer when carbon atoms are segregating from the substrate or when carbon atoms are deposited on top of the first graphene layer.[43] Further investigations of this growth process by using high-temperature STM or low-energy electron microscopy can potentially unveil

the role of C_{60} molecules in the formation of bilayer graphene on the Ir(111) surface and corresponding growth mechanism.

4. SUMMARY AND CONCLUSIONS

In summary, we have investigated the adsorption, electronic structure, and thermodynamics of C_{60} molecules on the Ir(111) and graphene/Ir(111) surfaces. We observed a strong interaction between C_{60} and the Ir surface in our STM measurements and DFT calculations. The strong interfacial interaction suppresses the diffusion of C_{60} molecules on the Ir surface, modifies their electronic structure via charge transfer, and leads to their decomposition at elevated temperatures. For the first time, we find that graphene can be formed on the Ir surface by thermal decomposition of C_{60}. The graphene interlayer attenuates the interaction of C_{60} molecules with the Ir surface, leading to a significant improvement in molecular self-assembly and the appearance of a zero-conductance gap. The observed effects of the graphene interlayer on the C_{60}/Ir interface provide rich and valuable information for designing molecule/metal interfaces for various potential applications.

■ ASSOCIATED CONTENT

⑤ Supporting Information

The Supporting Information is available free of charge on the ACS Publications website at DOI: 10.1021/acs.jpcc.5b09470.

> Spatial distribution of vacancies in C_{60} islands on the graphene/Ir(111) surface, the domain boundaries of graphene on the Ir(111) surface, the correlation between molecular arrangements and the domains on the underlying graphene/Ir(111) surface, the quantitative analysis of the dependence of the area of densely packed regions on the area of enclosed graphene islands, the intermediate structures between C_{60} and graphene during the growth of single- and bilayer graphene through thermal annealing of the C_{60}/Ir(111) surface, the calculated DOS of the C_{60} molecule on the Ir(111) and graphene/Ir(111) surfaces, and graphene patches obtained by thermal decomposition of C_2H_4 on the Ir(111) surface. (PDF)

■ AUTHOR INFORMATION

Corresponding Authors
*G.L.: E-mail: ganglu@csun.edu. Tel: 1-818-677-2021. Fax: 1-818-677-3234.
*L.G.: E-mail: li.gao@csun.edu. Tel: 1-818-677-4365. Fax: 1-818-677-3234.
Notes
The authors declare no competing financial interest.

■ ACKNOWLEDGMENTS

■ REFERENCES

(1) Park, H.; Park, J.; Lim, A. K. L.; Anderson, E. H.; Alivisatos, A. P.; McEuen, P. L. Nanomechanical Oscillations in a Single-C_{60} Transistor. *Nature* **2000**, *407*, 57−60.
(2) Winkelmann, C. B.; Roch, N.; Wernsdorfer, W.; Bouchiat, V.; Balestro, F. Superconductivity in a Single-C_{60} Transistor. *Nat. Phys.* **2009**, *5*, 876−879.

(3) Zhang, X.; Mizukami, S.; Kubota, T.; Ma, Q.; Oogane, M.; Naganuma, H.; Ando, Y.; Miyazaki, T. Observation of a Large Spin-Dependent Transport Length in Organic Spin Valves at Room Temperature. *Nat. Commun.* **2013**, *4*, 1392.

(4) Moorsom, T.; Wheeler, M.; Khan, T. M.; Ma'Mari, F. A.; Kinane, C.; Langridge, S.; Ciudad, D.; Bedoya-Pinto, A.; Hueso, L.; Teobaldi, G.; et al. Spin-Polarized Electron Transfer in Ferromagnet/C$_{60}$ Interfaces. *Phys. Rev. B: Condens. Matter Phys.* **2014**, *90*, 125311.

(5) Fei, X.; Wu, G.; Lopez, V.; Lu, G.; Gao, H.-J.; Gao, L. Spin-Dependent Conductance in Co/C$_{60}$/Co/Ni Single-Molecule Junctions in the Contact Regime. *J. Phys. Chem. C* **2015**, *119*, 11975−11981.

(6) Jariwala, D.; Sangwan, V. K.; Lauhon, L. J.; Marks, T. J.; Hersam, M. C. Carbon Nanomaterials for Electronics, Optoelectronics, Photovoltaics, and Sensing. *Chem. Soc. Rev.* **2013**, *42*, 2824−2860.

(7) Saran, R.; Stolojan, V.; Curry, R. J. Ultrahigh Performance C$_{60}$ Nanorod Large Area Flexible Photoconductor Devices via Ultralow Organic and Inorganic Photodoping. *Sci. Rep.* **2014**, *4*, 5041.

(8) Leary, R.; Westwood, A. Carbonaceous Nanomaterials for the Enhancement of TiO$_2$ Photocatalysis. *Carbon* **2011**, *49*, 741−772.

(9) Ward, P. A.; Teprovich, J. A.; Peters, B.; Wheeler, J.; Compton, R. N.; Zidan, R. Reversible Hydrogen Storage in a LiBH$_4$−C$_{60}$ Nanocomposite. *J. Phys. Chem. C* **2013**, *117*, 22569−22575.

(10) Cepek, C.; Goldoni, A.; Modesti, S. Chemisorption and Fragmentation of C$_{60}$ on Pt(111) and Ni(110). *Phys. Rev. B: Condens. Matter Phys.* **1996**, *53*, 7466−7472.

(11) Lu, J.; Yeo, P. S. E.; Gan, C. K.; Wu, P.; Loh, K. P. Transforming C$_{60}$ Molecules into Graphene Quantum Dots. *Nat. Nanotechnol.* **2011**, *6*, 247−252.

(12) Perdigão, L. M. A.; Sabki, S. N.; Garfitt, J. M.; Capiod, P.; Beton, P. H. Graphene Formation by Decomposition of C$_{60}$. *J. Phys. Chem. C* **2011**, *115*, 7472−7476.

(13) Yamada, Y.; Yamada, S.; Nakayama, T.; Sasaki, M.; Tsuru, T. Electronic Modificaiton of C$_{60}$ Monolayers via Metal Substrates. *Jpn. J. Appl. Phys.* **2011**, *50*, 08LB06.

(14) Zhang, X.; He, W.; Zhao, A.; Li, H.; Chen, L.; Pai, W. W.; Hou, J.; Loy, M. M. T.; Yang, J.; Xiao, X. Geometric and Electronic Structure of a C$_{60}$ Monolayer on Ag(100). *Phys. Rev. B: Condens. Matter Phys.* **2007**, *75*, 235444.

(15) Altman, E. I.; Colton, R. J. Nucleation, Growth, and Structure of Fullerene Films on Au(111). *Surf. Sci.* **1992**, *279*, 49−67.

(16) Weckesser, J.; Cepek, C.; Fasel, R.; Barth, J. V.; Baumberger, F.; Greber, T.; Kern, K. Binding and Ordering of C$_{60}$ on Pd(110): Investigations at the Local and Mesoscopic Scale. *J. Chem. Phys.* **2001**, *115*, 9001−9009.

(17) Cho, J.; Gao, L.; Tian, J.; Cao, H.; Wu, W.; Yu, Q.; Yitamben, E. N.; Fisher, B.; Guest, J. R.; Chen, Y. P.; Guisinger, N. P. Atomic-Scale Investigation of Graphene Grown on Cu Foil and the Effects of Thermal Annealing. *ACS Nano* **2011**, *5*, 3607−3613.

(18) Chen, S.; Brown, L.; Levendorf, M.; Cai, W.; Ju, S.-Y.; Edgeworth, J.; Li, X.; Magnuson, C. W.; Velamakanni, A.; Piner, R. D.; et al. Oxidation Resistance of Graphene-Coated Cu and Cu/Ni Alloy. *ACS Nano* **2011**, *5*, 1321−1327.

(19) Krishnamurthy, A.; Gadhamshetty, V.; Mukherjee, R.; Chen, Z.; Ren, W.; Cheng, H.-M.; Koratkar, N. Passivation of Mirobial Corrosion Using a Graphene Coating. *Carbon* **2013**, *56*, 45−49.

(20) Singh Raman, R. K.; Tiwari, A. Graphene: The Thinnest Known Coating for Corrosion Protection. *JOM* **2014**, *66*, 637−642.

(21) Balandin, A. A. Thermal Properties of Graphene and Nanostructured Carbon Materials. *Nat. Mater.* **2011**, *10*, 569−581.

(22) Xu, X.; Pereira, L. F. C.; Wang, Y.; Wu, J.; Zhang, K.; Zhao, X.; Bae, S.; Bui, C. T.; Xie, R.; Thong, J. T. L.; et al. Length-Dependent Thermal Conductivity in Suspended Single-Layer Graphene. *Nat. Commun.* **2014**, *5*, 3689.

(23) Pop, E.; Varshney, V.; Roy, A. K. Thermal Properties of Graphene: Fundamentals and Applications. *MRS Bull.* **2012**, *37*, 1273−1281.

(24) Goli, P.; Ning, H.; Li, X.; Lu, C. Y.; Novoselov, K. S.; Balandin, A. A. Thermal Properties of Graphene-Copper-Graphene Heterogeneous Films. *Nano Lett.* **2014**, *14*, 1497−1503.

(25) Rho, H.; Lee, S.; Bae, S.; Kim, T.-W.; Lee, D. S.; Lee, H. J.; Hwang, J. Y.; Jeong, T.; Kim, S.; Ha, J.-S.; et al. Three-Dimensional Porous Copper-Graphene Heterostructures with Durability and High Heat Dissipation Performance. *Sci. Rep.* **2015**, *5*, 12710.

(26) Zhou, H. T.; Mao, J. H.; Li, G.; Wang, Y. L.; Feng, X. L.; Du, S. X.; Müllen, K.; Gao, H.-J. Direct Imaging of Intrinsic Molecular Orbitals Using Two-Dimensional, Epitaxially-Grown, Nanostructured Graphene for Study of Single Molecule and Interactions. *Appl. Phys. Lett.* **2011**, *99*, 153101.

(27) Cho, J.; Smerdon, J.; Gao, L.; Süzer, Ö.; Guest, J. R.; Guisinger, N. P. Structural and Electronic Decoupling of C$_{60}$ from Epitaxial Graphene on SiC. *Nano Lett.* **2012**, *12*, 3018−3024.

(28) Uihlein, J.; Peisert, H.; Adler, H.; Glaser, M.; Polek, M.; Ovsyannikov, R.; Bauer, M.; Chassé, T. Strong Interaction of MnPc on Ni(111): Influence of Graphene Buffer Layer. *J. Phys. Chem. C* **2014**, *118*, 28671−28678.

(29) Uihlein, J.; Peisert, H.; Glaser, M.; Polek, M.; Adler, H.; Petraki, F.; Ovsyannikov, R.; Bauer, M.; Chassé, T. Communication: Influence of Graphene Interlayers on the Interaction between Cobalt Phthalocyanine and Ni(111). *J. Chem. Phys.* **2013**, *138*, 081101.

(30) Uihlein, J.; Peisert, H.; Adler, H.; Glaser, M.; Polek, M.; Ovsyannikov, R.; Chassé, T. Interface between FePc and Ni(111): Influence of Graphene Buffer Layers. *J. Phys. Chem. C* **2014**, *118*, 10106−10112.

(31) Pletikosić, I.; Kralj, M.; Pervan, P.; Brako, R.; Coraux, J.; N'Diaye, A. T.; Busse, C.; Michely, T. Dirac Cones and Minigaps for Graphene on Ir(111). *Phys. Rev. Lett.* **2009**, *102*, 056808.

(32) Shi, X.-Q.; Van Hove, M.; Zhang, R.-Q. Survey of Structural and Electronic Properties of C$_{60}$ on Close-Packed Metal Surfaces. *J. Mater. Sci.* **2012**, *47*, 7341−7355.

(33) Kresse, G.; Furthmüller, J. Efficient Iterative Schemes for Ab Initio Total-Energy Calculations Using a Plane-Wave Basis Set. *Phys. Rev. B: Condens. Matter Phys.* **1996**, *54*, 11169−11186.

(34) Blöchl, P. E. Projector Augmented-Wave Method. *Phys. Rev. B: Condens. Matter Phys.* **1994**, *50*, 17953−17979.

(35) Perdew, J. P.; Burke, K.; Ernzerhof, M. Generalized Gradient Approximation Made Simple. *Phys. Rev. Lett.* **1996**, *77*, 3865−3868.

(36) Grimme, S. Semiempirical GGA-type Density Functional Constructed with a Long-range Dispersion Correction. *J. Comput. Chem.* **2006**, *27*, 1787−1799.

(37) Bokareva, O. S.; Kuhn, O. DFT-D Investigation of the Interaction between Ir (111) based Photosensitizers and Small Silver Clusters Ag$_n$ (*n* = 2−20, 92). *Chem. Phys.* **2014**, *435*, 40−48.

(38) Li, G.; Zhou, H. T.; Pan, L. D.; Zhang, Y.; Mao, J. H.; Zou, Q.; Guo, H. M.; Wang, Y. L.; Du, S. X.; Gao, H.-J. Self-Assembly of C$_{60}$ Monolayer on Epitaxially Grown, Nanostructured Graphene on Ru(0001) Surface. *Appl. Phys. Lett.* **2012**, *100*, 013304.

(39) Gao, L. Probing Electronic Properties of Graphene on the Atomic Scale by Scanning Tunneling Microscopy and Spectroscopy. *Graphene 2D Mater.* **2014**, *1*, 23−46.

(40) Gao, L.; Guest, J. R.; Guisinger, N. P. Epitaxial Graphene on Cu(111). *Nano Lett.* **2010**, *10*, 3512−3516.

(41) Yu, G.; Gao, J.; Hummelen, J. C.; Wudl, F.; Heeger, A. J. Polymer Photovoltaic Cells: Enhanced Efficiencies Via a Network of Internal Donor-Acceptor Heterojunctions. *Science* **1995**, *270*, 1789−1791.

(42) Berland, K.; Hyldgaard, P. Analysis of Van Der Waals Density Functional Components: Binding and Corrugation of Benzene and C$_{60}$ on Boron Nitride and Graphene. *Phys. Rev. B: Condens. Matter Phys.* **2013**, *87*, 205421 .

(43) Nie, S.; Walter, A. L.; Bartelt, N. C.; Starodub, E.; Bostwick, A.; Rotenberg, E.; McCarty, K. F. Growth from Below: Graphene Bilayers on Ir(111). *ACS Nano* **2011**, *5*, 2298−2306.